Electroencephalography Study of Frontal Lobe Evoked by Dynamic Random-Dot Stereogram

Yueping Li,[1] Lili Shen,[2] and Mingyang Sun[2]

[1]Pediatric Ophthalmology and Strabismus Department, Tianjin Eye Hospital, Clinical College of Ophthalmology of Tianjin Medical University, Tianjin Key Laboratory of Ophthalmology and Vision Science, Tianjin, China
[2]School of Electronic Information Engineering, Tianjin University, Tianjin, China

Correspondence: Yueping Li, Pediatric Ophthalmology and Strabismus Department, Tianjin Eye Hospital, Clinical College of Ophthalmology of Tianjin Medical University, Tianjin Key Laboratory of Ophthalmology and Vision Science, Tianjin 300020, China; leeyueping@aliyun.com.

Received: December 1, 2021
Accepted: April 13, 2022
Published: May 6, 2022

Citation: Li Y, Shen L, Sun M. Electroencephalography study of frontal lobe evoked by dynamic random-dot stereogram. *Invest Ophthalmol Vis Sci.* 2022;63(5):7. https://doi.org/10.1167/iovs.63.5.7

Purpose. The purpose of this study was to investigate the cortical electrical activity and electroencephalography (EEG) features of the frontal lobe evoked by dynamic random dot stereogram (DRDS) and to probe the functional connectivity (FC) between the frontal lobe and occipital lobe when processing 3D perception based on the binocular disparity.

Methods. The EEG experiment involved 14 healthy adults with normal stereopsis (<60″) and normal corrected visual acuity (20/20). The Neuroscan system and 32-channel EEG cap were used to record EEG signals based on the DRDS stimuli. The maximum energies of 3 frequency bands (theta-/alpha- /beta-wave) from 13 interesting channels (FP1, FP2, F7, F3, FZ, F4, F8, FC3, FCZ, FC4, O1, OZ, and O2) located in the frontal and occipital lobes were calculated and analyzed. The FC between any two electrodes from the frontal and occipital lobes was calculated based on the Phase lag index (PLI).

Results. The maximum powers of theta- and alpha-waves in most channels of the frontal and occipital lobes were significantly increased ($P < 0.05$) when the depth perception was evoked by DRDS above the threshold, compared with that without stereo vision. The changes in the maximum powers of both theta- and alpha-waves were significantly different among the 13 electrodes ($P = 0.0004$ and 0.0015, respectively). Tukey's multiple comparisons showed that the changes in the maximum powers of theta-wave were significantly different in F8 vs. O1, F8 vs. OZ, and F4 vs. O1 ($P = 0.0186$, 0.0444, and 0.0412, respectively). Moreover, the changes in the maximum powers of alpha-waves were significantly different in FP1 vs. O1 ($P = 0.0182$). The FCs of theta-waves between the frontal channels and the occipital channels were significantly enhanced when processing the depth perception, compared with those without stereopsis. There was no significant change in the FCs of the alpha-waves when having 3D perception except for FC between F8 and O1 and FC between F8 and OZ.

Conclusions. The cortical electrical activity in the frontal lobe and the functional connectivity between the frontal lobe and the occipital lobe increase when participating in the processing binocular disparity and obtaining 3D perception. Theta-waves in the frontal lobe may be crucial in the stereo vision.

Keywords: dynamic random dot stereogram (DRDS), electroencephalograph (EEG), stereopsis, frontal lobe, functional connectivity (FC)

Stereopsis, known as the 3D perception, is an advanced binocular vision function based on binocular simultaneous perception and fusion. Binocular relative parallax is the basis of producing fine stereopsis. Fine parallax may also be involved in accomplishing the ocular vergence and the maintaining the binocular fixation.[1] The neurons of primary visual cortex (V1) participate in the early processing of binocular disparity and then send axons to extrastriate areas (V2 and V3).[1–3] Then, the visual pathway separates the ventral and the dorsal streams. The classic theory indicates that the dorsal visual pathway runs from the occipital lobe to the parietal lobe and processes motor and spatial information and rough depth perception.[4,5] The ventral pathway, called the occipital-temporal pathway, is crucial for the visual recognition of objects.[6] The neuronal electrophysiological studies and functional magnetic resonance imaging (fMRI) studies have confirmed the presence of parallax-sensitive neurons in the occipital, temporal, and parietal lobes.

Frontal lobes have at least five subcortical regions: supplementary motor area (SEF), frontal eye fields (FEFs), dorsolateral prefrontal cortex (DLPFC), orbitofrontal cortex, and anterior cingulate cortex.[7] Frontal lobes are reciprocally connected with temporal, parietal, and occipital lobes.[8–10] FEFs participate in the initiation and maintenance of various eye movements, including gaze,[8] saccades,[11] pursuit,[12,13] and vergence eye movement.[14] Most of the neurons in FEFs are sensitive to retinal disparity and have a broad depth tuning for near or far disparity.[14] FEFs are also sensitive to the velocity of motion-in-depth.[15] Therefore, the frontal lobe is deemed to participate in the initiation of disconjugate eye movements, including convergence and divergence.

The random dots stereogram (RDS) invented by Julesz only provides binocular parallax cues to generate figures that are visible after binocular fusion and eliminate the monocular clues.[16] RDS is widely used in clinical examination and the stereoscopic cognition field. Electroencephalogram (EEG), as a noninvasive acquisition, is commonly used in stereo vision cognition to collect the activities of the cerebral cortex. An EEG can record brain activity and reflect the physiological phenomenon stimulated by RDS.[17,18]

In our previous study, we developed the dynamic random-dot stereograms (DRDS) to probe characteristics of the EEG evoked by DRDS video. That study showed that two visual streams had certain neural connection and were usually simultaneously activated during recognition.[19,20] This study aimed to assess the EEG features of frontal lobes and functional connectivity (FC) between frontal lobes and occipital lobes evoked by DRDS.

Materials and Methods

Participants

A total of 14 healthy young adults (7 male and 7 female participants, aged 20–25 years) took part in the study. The study was approved by the institutional review board of Tianjin Eye Hospital and followed the tenets of the Declaration of Helsinki. Informed consents were obtained from all the participants.

Exclusion criteria were: participants with strabismus, nystagmus, anisometropia or other ocular diseases causing deficiency of binocular vision. All the subjects had normal corrected visual acuity (20/20) and 40" to 60 stereopsis based on the Titmus test.

Apparatus

The skin of the participants was cleaned before the placement of electrodes according to the international registration system 10-20.[21] A brain-computer interface (BCI) experimental platform was used to collect and process EEG data, as shown in Figure 1. EEG signals were collected by an embedded 32-channel EEG cap and Neuroscan system. The frontal lobe and occipital lobe were the regions of interest (ROI). Thirteen EEG electrodes in ROI as the interested electrodes, including FP1, FP2, F7, F3, FZ, F4, F8, FC3, FCZ, FC4, O1, OZ, and O2, were placed as shown in Figure 1.

EEG Experiment

Stimulation and Procedure. The DRDS video generated by MATLAB was used as the experimental stimulus. A 3D object with a graphic (square, rectangle, circle, or oval) in the DRDS periodically moved back and forth at the center of the screen. There were 22 types of stereoscopic videos with parallax ranging from 5″ to 100″ with a step size of 5″, together with parallax 200″, 300″, and the duration time is 4 seconds. The whole experiment presented by E-prime was divided into three subsessions with each type of video randomly presented four times in each subsession.

Participants were seated 102 cm from the screen and gave feedback the shapes of the graphics using the keyboard for each trial while watching the DRDS videos. During the trials, the participants were required to sit up straight and keep their heads stable. At the end of each subsession, the participant took a rest for 2 minutes.

The stereoscopic parallax curve was fitted according to the correct detection rate for the stereoscopic acuity determination. The stereoscopic acuity values of the DRDS ranged from 40″ to 50″ in all the subjects. Two disparities of DRDS were selected as EEG stimulus, including 20″ (unperceived totally, as condition 1) and 100″ (perceived clearly, as condition 2).

The participants were asked to avoid consumption of alcohol, coffee, drugs, or other substances which could affect their mental state 24 hours before the EEG experiment. After understanding the purpose of the experiment and relevant contents, the participants sat 102 cm from the screen in a dimly lit room and watched a moving 3D graphic wearing the EEG cap. The participants focused on a cross image displayed on the center of the screen for 0.5 seconds at the beginning of each trail. A DRDS video then appeared and lasted for 4 seconds. The participants were required to recognize the shape in mind. The participants remained sitting up straight and stable and silent without any moving during the experiment. The completed experiment consisted of 6 subsessions and each subsession contained 48 trials. In total, eight conditions, including four graphics with two different cross parallaxes, were randomly shown six times in each subsession. There was a 1 second rest between the two trials and at least a 2 minute rest after each subsection.

Signal Analysis and Data Collection Process. For electro-oculogram (EOG) signal monitoring, a bipolar channel was placed on the left and right temples for horizontal EOG and another one was placed above and below the left

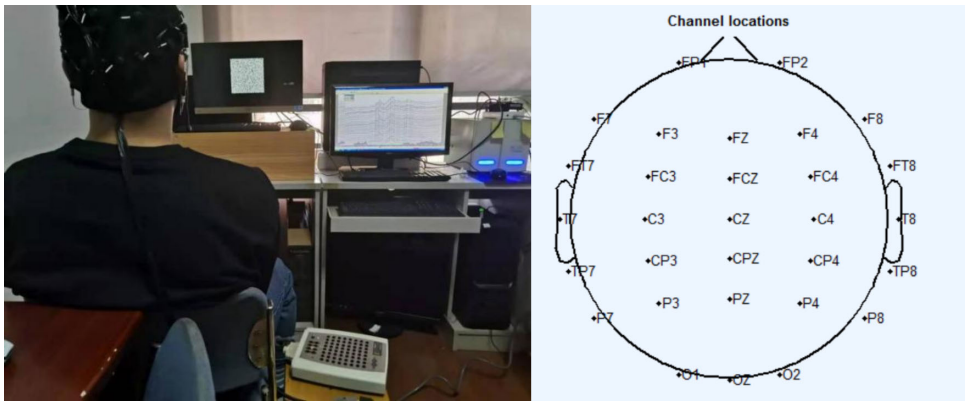

Figure 1. The experimental device and electrode positions.

Investigative Ophthalmology & Visual Science

eye for vertical EOG. The left mastoid process was used as the reference electrode and impedance of each channel was kept below 5 kΩ. EEG signals were collected at the sampling frequency of 1000 Hz and analyzed using MATLAB.

Signal Preprocessing. An EEGLAB tool kit in MATLAB was used to reduce the artifacts and preprocess EEG data. EEG signals were categorized based on frequency ranges, which were theta-wave (4–8 Hz), alpha-wave (8–12 Hz), and beta-wave (12–30 Hz). Signal preprocessing was conducted as follows: (1) loading of the raw data; (2) filtering: the EEG signals passed through the finite impulse response (FIR) high-pass filter at 1 Hz and the FIR low-pass fifilter at 30 Hz to eliminate low-frequency DC components and other artifact noise at high frequencies; (3) splitting of the entire data into segments every 4 seconds; and (4) removing EOG and EMG through independent component analysis (ICA).

Calculation and Analysis of Maximum Energy of the Channels From the ROI. We calculated the maximum energy/power of three waves (theta-, alpha- and beta-waves) in 4 seconds (DRDS video presenting) of each interesting electrode (FP1, FP2, F7, F3, FZ, F4, F8, FC3, FCZ, FC4, O1, OZ, and O2) in condition 1 and in condition 2. The baseline correction was performed for each subject using the corresponding energy at 100 ms before stimulation. The formula is as follows:

$$E_{kj} = max(|X_{kj}(i)|^2)$$

(j=1, 2, and 3 represents the θ, α, and β frequency band, respectively; k represents the channel label (Fig. 1); E_{kj}, represents the maximum energy of j frequency band from the k channel; $X_{kj}(i)$, represents the signal amplitude at i sampling point from the j frequency band on the k channel).

Calculation and Analysis of the Functional Connectivity of the Channels Among ROI. FC is a temporally associated activity in the brain regions. As a novel measure to quantify phase synchronization, phase lag index (PLI) reflects the consistency of a signal relative to the phase advance or lag of the other signal. PLI is calculated as follows:

$$PLI = |\langle sign(\Delta\phi_{rel}(t))\rangle| = \left|\frac{1}{N}\sum_{n=1}^{N} sign(\Delta\phi_{rel}(t_n))\right|$$

PLI values range between 0 and 1. PLI performs well in detecting the real change of synchronization in brain networks because it is invariant to volume conduction.[22,23] Herein, PLI was used to calculate the FC between two channels in our study.

Statistical Analysis

Statistical analyses were carried out using SPSS Statistics 22.0 (IBM, Armonk, NY, USA). The t-paired test was used to analyze and compare the maximum powers of theta-, alpha-, and beta-waves in each channel between the two conditions. The FCs between any two channels in condition 1 and condition 2 were also compared using the t-paired test. ANOVA was used to detect the changes of the maximum powers of the three waves among all the electrodes and then Tukey's multiple comparisons test was used if there was significant difference. ANOVA was also used to analyze the changes of maximal powers in each electrode among the three waves. The confidence interval (CI) used in this study was 95% with an alpha of 0.05 (a = 0.05).

Results

The Maximal Powers of Theta-\Alpha-\Beta-Waves of the Interesting Channels in Condition 1 and Condition 2

The maximal powers of theta-, alpha-, and beta-waves of the interesting channels in condition 1 and condition 2 were shown in the Table 1 and Figure 2. When subjects had stereo vision, the maximal powers of theta-wave significantly increased in 13 electrodes (FP1, FP2, F7, F3, FZ, F4, F8, FC3, FCZ, FC4, O1, Oz, and O2), compared with those when no stereo vision. Comparing the maximal powers of the alpha-waves between two conditions, there were significant differences in 11 electrodes (FP1, FP2, F7, F3, FZ, F4, F8, FC3, FCZ, FC4 and O2). The maximal powers of beta-wave significantly increased in 8 channels (FP1, FP2 F7, FZ, F4, F8, O1, Oz) in condition 2.

There were significant differences in the changes of the maximal powers among theta-, alpha-, and beta-waves in nine electrodes (FP1, FP2, F3, FZ, F4, FC3, FCZ, FC4, and O2; Table 2. and Fig. 3a). The maximal powers of the theta-waves significantly increased in the above channels. Moreover, there were significant differences in the changes of maximal powers of theta-wave (ANOVA analysis, F = 2.973,

Table 1. The Maximal Powers (μV^2) of Theta-\Alpha-\Beta-Waves of the Interesting Channels in Condition 1 and Condition 2

	Theta-Wave				Alpha-Wave				Beta-Wave			
	Condition 1	Condition 2	*t*	*P*	Condition 1	Condition 2	*t*	*P*	Condition 1	Condition 2	*t*	*P*
FP1	4.80 ± 4.03	9.50 ± 5.01	8.953	0.001	1.61 ± 1.24	3.62 ± 1.84	4.990	0.001	0.25 ± 0.17	0.48 ± 0.34	2.690	0.018
FP2	5.58 ± 5.19	9.94 ± 5.82	7.577	0.001	1.84 ± 1.55	3.65 ± 1.94	5.180	0.001	0.27 ± 0.17	0.60 ± 0.33	4.033	0.001
F7	2.64 ± 2.08	7.72 ± 5.88	3.123	0.008	0.94 ± 0.73	2.54 ± 1.67	3.471	0.004	0.17 ± 0.09	0.25 ± 0.10	2.353	0.035
F3	2.80 ± 1.98	7.85 ± 3.49	5.262	0.001	1.00 ± 0.61	2.52 ± 1.00	5.891	0.001	0.23 ± 0.13	0.37 ± 0.25	2.146	0.051
FZ	2.96 ± 2.77	8.52 ± 3.93	5.996	0.001	1.08 ± 0.84	2.68 ± 1.09	6.965	0.001	0.26 ± 0.13	0.31 ± 0.17	2.285	0.040
F4	2.87 ± 2.37	8.60 ± 4.02	5.259	0.001	1.05 ± 0.71	2.67 ± 1.06	5.895	0.001	0.22 ± 0.10	0.30 ± 0.13	3.500	0.004
F8	2.35 ± 1.73	8.41 ± 8.11	2.766	0.016	0.80 ± 0.56	2.63 ± 2.32	2.907	0.012	0.15 ± 0.07	0.28 ± 0.14	4.140	0.001
FC3	2.23 ± 1.64	5.98 ± 2.66	6.849	0.001	0.81 ± 0.49	1.95 ± 0.83	7.545	0.001	0.25 ± 0.15	0.37 ± 0.31	1.784	0.098
FCZ	2.58 ± 2.87	6.75 ± 3.72	8.637	0.001	0.92 ± 0.85	2.19 ± 1.25	7.563	0.001	0.26 ± 0.19	0.42 ± 0.36	2.023	0.064
FC4	2.59 ± 2.17	7.08 ± 3.15	5.713	0.001	1.00 ± 0.87	2.21 ± 0.89	5.512	0.001	0.22 ± 0.12	0.40 ± 0.36	2.118	0.054
O1	2.80 ± 2.98	3.82 ± 2.83	2.460	0.029	1.25 ± 1.67	1.56 ± 1.47	0.802	0.437	0.29 ± 0.38	0.58 ± 0.65	3.420	0.005
OZ	2.22 ± 1.89	3.60 ± 2.88	3.759	0.002	0.94 ± 0.95	1.52 ± 1.59	2.052	0.061	0.31 ± 0.45	0.47 ± 0.49	2.271	0.041
O2	1.98 ± 1.75	3.88 ± 3.35	4.121	0.001	0.85 ± 0.92	1.50 ± 1.40	3.552	0.004	0.34 ± 0.49	0.48 ± 0.46	1.947	0.073

Investigative Ophthalmology & Visual Science

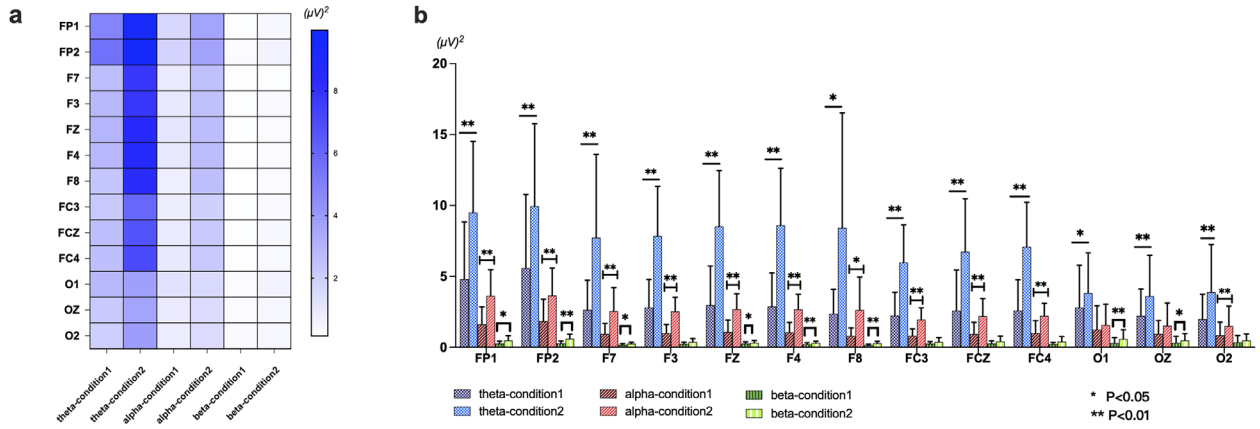

Figure 2. The maximal power of theta-, alpha- and beta-waves of 13 electrodes of ROI in condition 1 (20″, unperceived totally) and condition 2 (100″, perceived clearly). (**a**) Heat map; (**b**) summary data and ANOVA analysis.

Table 2. The Changes of Maximal Powers (μV^2) of Theta-, Alpha-, and Beta-Waves in the Interesting Electrodes

	Theta	Alpha	Beta	F	*P* Value
FP1	4.70 ± 2.04	2.01 ± 1.57	0.22 ± 0.32	35.05	0.0002
FP2	4.37 ± 2.24	1.81 ± 1.36	0.33 ± 0.32	22.39	0.0011
F7	5.08 ± 6.34	1.60 ± 1.79	0.08 ± 0.14	4.386	0.081
F3	5.05 ± 3.74	1.52 ± 1.01	0.16 ± 0.26	11.87	0.0131
FZ	5.56 ± 3.61	1.60 ± 0.90	0.05 ± 0.09	15.97	0.007
F4	5.73 ± 4.24	1.63 ± 1.07	0.08 ± 0.09	12.17	0.0128
F8	6.06 ± 8.53	1.83 ± 2.45	0.13 ± 0.12	3.424	0.1136
FC3	3.74 ± 2.13	1.14 ± 0.59	0.12 ± 0.27	18.84	0.0041
FCZ	4.17 ± 1.88	1.27 ± 0.65	0.16 ± 0.31	30.92	0.001
FC4	4.49 ± 3.06	1.22 ± 0.86	0.18 ± 0.33	13.51	0.009
O1	1.02 ± 1.61	0.32 ± 1.54	0.29 ± 0.33	1.124	0.3445
OZ	1.39 ± 1.43	0.59 ± 1.11	0.16 ± 0.27	4.447	0.0629
O2	1.90 ± 1.80	0.65 ± 0.72	0.13 ± 0.26	5.68	0.0482

$P = 0.0004$) and alpha band (F = 2.642, $P = 0.0015$) among the 13 interesting electrodes (Fig. 3b). In contrast, the changes of maximal powers of beta-wave were not significantly different among 13 interesting electrodes (F = 1.503, $P = 0.1126$). Further, by the Tukey's multiple comparisons tests it showed that the changes of maximal powers of theta-wave were significantly different in F8 vs. O1, F8 vs. OZ, and F4 vs. O1 ($P = 0.0186$, 0.0444, and 0.0412, respectively; Fig. 3c). The changes of the maximal powers of the alpha-waves were significantly different only in FP1 vs. O1 ($P = 0.0182$; Fig. 3d).

Functional Connectivity of Theta and Alpha-Frequency Band

PLI was used to calculate the FC between any two electrodes in the ROI. The PLI values of the theta-waves in condition 1

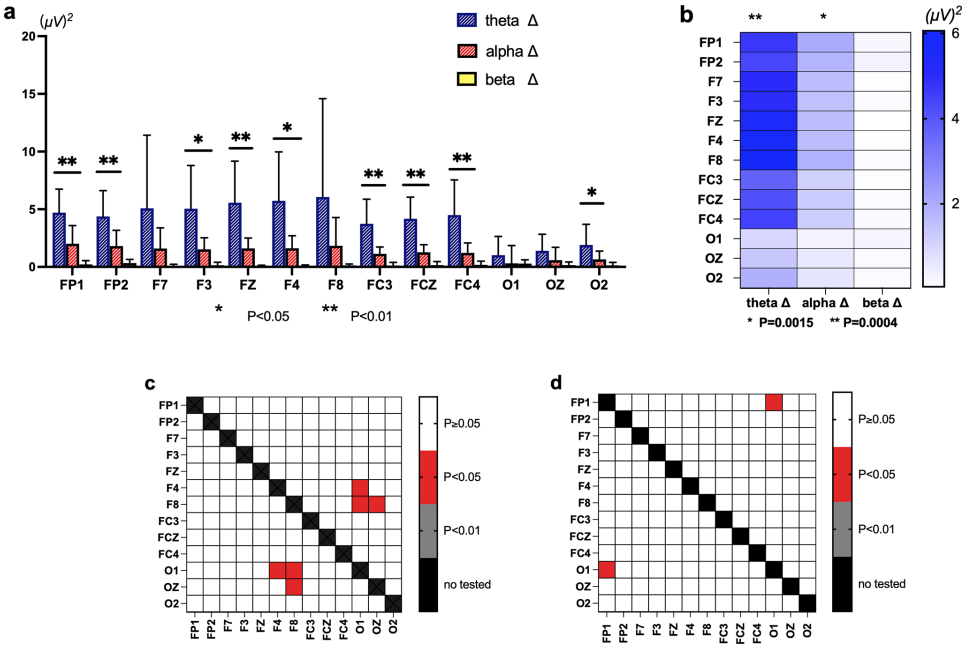

Figure 3. The changes (Δ) of maximal powers of theta-, alpha-, and beta-waves of the 13 electrodes in the ROI induced by depth perception. (**a, b**) The Δ maximal powers of theta-, alpha-, and beta-waves in all the electrodes. (**c**) Grid of Tukey's multiple comparisons of Δ maximal powers of the theta-waves. (**d**) Grid of Tukey's multiple comparisons of Δ maximal powers of the alpha-waves.

Investigative Ophthalmology & Visual Science

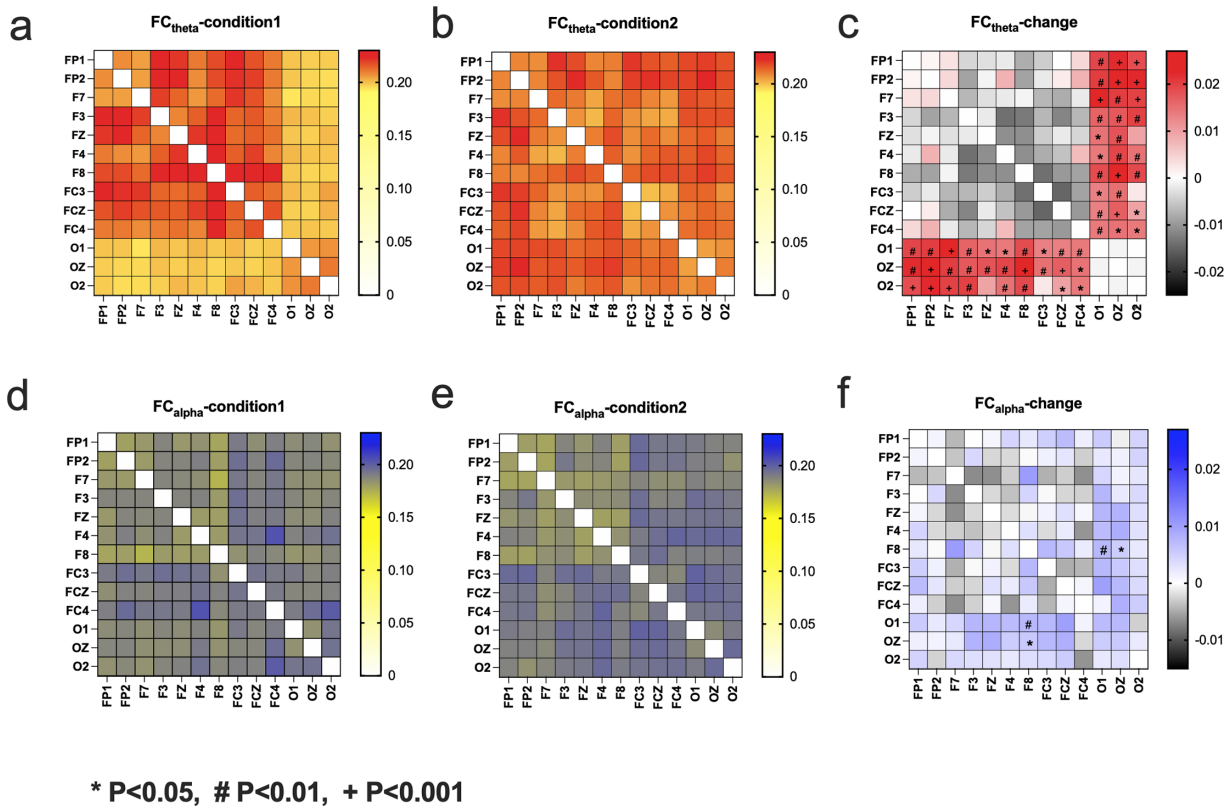

Figure 4. Functional connectivity of theta and alpha-waves between any two channels among the interesting electrodes from the frontal lobe and occipital lobe. (**a**) The PLI values of theta-wave under condition 1 (20″, unperceived totally). (**b**) The PLI values of the theta-waves under condition 2 (100″, perceived clearly). (**c**) The FC changes of the theta-waves and the comparisons between FCs in condition 2 and those in condition 1. (**d**) The PLI values of the alpha-waves under condition 1. (**e**) The PLI values of the alpha-waves under condition 2. (**f**) The FC changes of the alpha-waves and the comparisons between FCs in condition 2 and those in condition 1 (* $P < 0.05$, # $P < 0.01$, + $P < 0.001$).

are shown in Figure 4a and those in condition 2 are shown in Figure 4b, respectively. The FC changes of the theta-waves between any two electrodes were presented in Figure 4c, which were defined as the PLI value in condition 2 minus that in condition 1. The FCs of the theta-waves between the electrodes from the frontal lobe and those from the occipital lobe were significantly enhanced in condition 2, compared with those in condition 1 (see Fig. 4c, * $P < 0.05$, # $P < 0.01$, + $P < 0.001$).

The PLI values of the alpha-waves in condition 1 are shown in Figure 4d and those in condition 2 are shown in Figure 4e. The FC changes of the alpha-waves between any two electrodes are presented in Figure 4f. Only FC of the alpha-waves between F8 and O1 and FC between F8 and OZ were significantly enhanced in condition 2 (Fig. 4f, * $P < 0.05$, # $P < 0.01$, + $P < 0.001$).

Discussion

The visual pathway separates the ventral stream and the dorsal stream, also called as the occipital-parietal pathway and occipital-temporal pathway. The neuronal electrophysiological studies and fMRI studies confirm the presence of parallax-sensitive neurons in both visual pathways.[24] Binocular vision and stereoscopic depth perception are essential in daily life, such as eye–hand coordination.[25,26] Patients with abnormal binocular vision have impairments in reaching and grasping hand movements.[27,28]

The frontal lobes are reciprocally connected with temporal, parietal, and occipital lobes.[8–10,29] The frontal lobe participates in initiation and maintenance of various eye movements to maintain the binocular fusion.[2] Most of the neurons in the FEFs are sensitive to retinal disparity and broadly tuned in depth for near or far disparity.[15] The FEFs were also sensitive to the velocity of motion-in-depth.[30] Furthermore, visual information processing is associated with ocular motility control and visual attention, which is influenced by top-down regulation of the frontal-parietal cortex. Abnormal visual development can change the top-down regulation from the frontal lobe to the occipital lobe.[31] EEG experiments have shown that the frontal lesions can cause the deficits in top-down modulation of activity in visual extrastriate cortex during attention.[32,33] The reduced FC among the frontal, parietal, and occipital regions cause the deficits of visuomotor and visual-guided actions.[34,35]

However, the cortical electrical activity of the frontal lobe and the FC between the frontal and occipital lobes evoked by binocular disparity in normal humans is unknown. In our previous study, DRDS was developed to investigate the characteristics of EEG evoked by DRDS. We found both dorsal and ventral streams were simultaneously activated in the process of recognition of 3D shapes embedded in DRDS and there was a certain neural connection between them.[19,20] Herein, two disparities of DRDS were used in this study, which were below and above the threshold. Definitely, only the latter could generate stereo vision in the

Investigative Ophthalmology & Visual Science

healthy subjects. Our findings showed that the activities of theta-waves and alpha-waves in all the frontal lobe were significantly increased when the subjects obtained stereopsis evoked by the binocular disparity above the threshold. Although there were differences in the changes of the maximum powers among the interesting channels, there was no difference between mostly frontal electrodes and the occipital electrodes analyzed by multiple comparisons test. The functional connectivity of the theta-waves significantly increased between the frontal and occipital lobes when the subject had 3D perception. The increasing activity of the theta-waves in the frontal lobe was correlated with activity of the occipital lobe. These findings indicate that the frontal lobe participates in the process of recognition of 3D shapes embedded in RDS. The specific changes in the frontal lobe may also be related to the regulation of binocular movements when watching DRDS. Although the activity of the theta-waves increased in the occipital lobe, the activity of the alpha-waves was not significantly different between processing binocular disparity below the threshold and that above the threshold. The roles of the different waves should be further studied. Cumming and Parker suggested that disparity selective neurons in the primary visual cortex were not associated with stereoscopic cognition, which involved higher level areas of the cortical network from binocular cues.[36] We found there was no asymmetry of the theta-, alpha-, and beta-waves' activities in the ROI and FC between the frontal and occipital regions in the cerebral hemispheres.

The alpha-wave is found in the posterior and occipital regions of healthy subjects in the waking-state.[37] Lower alpha-wave activity and abnormal distribution of theta-waves in the frontal lobes are found in strabismus and amblyopia, which is related with neurodevelopmental disorders.[38] However, a few studies have explored the function of the advanced cortex in the task-state of 3D perception evoked by DRDS. Our study showed the cortical activity of the theta-waves significantly changed in the frontal lobe of healthy adults when processing binocular disparity. The resting-state fMRI studies showed the enhanced activation of bilateral parietal,[39] specific frequency domain amplitude of low frequency fluctuation (ALFF) changes in the right outer occipital complex in intermittent exotropia.[40] Therefore, we suggested that the frontal region function in the task-state should be further investigated in the patients with abnormal binocular vision.

In conclusion, this study demonstrated the specific features of EEG in the frontal and occipital lobes and FC between the frontal and occipital lobes, which were definitely associated with binocular disparity. Theta-wave activity in the frontal lobe might be predominant in the stereoscopic perception.

Acknowledgments

Supported by Tianjin Key Medical Discipline (Specialty) Construction. Science and Technology Project of Tianjin Health Commission (ZC20187), and Science and Technology Found of Tianjin Eye Hospital (YKZD2001).

Disclosure: **Y. Li**, None; **L. Shen**, None; **M. Sun**, None

References

1. Poggio GF. Mechanisms of stereopsis in monkey visual cortex. *Cereb Cortex*. 1995;5:193–204.
2. Poggio GF, Fisher B. Binocular interaction and depth sensitivity in striate and prestriate cortex of behaving rhesus monkey. *J Neurophysiol*. 1977;40:1392–1405.
3. Roe AW, Parker AJ, Born RT, DeAngelis GC. Disparity channels in early vision. *J Neurosci*. 2007;27(44):11820–11831.
4. Perry CJ, Fallah M. Feature integration and object representations along the dorsal stream. *Front Computat Neuroscie*. 2014;8(18):84.
5. Nadler JW, Angelaki DE, DeAngelis GC. A Neural Representation of Depth from Motion Parallax in Macaque Visual Cortex. *Nature*. 2008;452(7187):642–645.
6. Verhoef BE, Vogels R, Janssen P. Binocular depth processing in the ventral visual pathway Phil. *Trans R Soc B*. 2016;371:20150259.
7. Cummings JL. Frontal-subcortical circuits and human behavior. *Arch Neurol*. 1993;50(8):873–880.
8. Schall JD. Visuomotor Functions in the Frontal Lobe. *Annu Rev Vis Sci*. 2015;1:469–498.
9. Barbas H. Architecture and cortical connections of the prefrontal cortex in the rhesus monkey. *Adv Neurol*. 1992;57:91–115.
10. Cavada C, Goldman-Rakic PS. Posterior parietal cortex in rhesus monkeys: II. Evidence for segregated corticocortical networks linking sensory and limbic areas with the frontal lobes. *J Comp Neurol*. 1989;287:422–445.
11. Gamlin PD, Yoon K. An area for vergence eye movement in primate frontal cortex. *Nature*. 2000;407 (6807):1003–1007.
12. Fukushima K, Yamanobe T, Shinmei Y, Fukushima J, Kurkin S, Peterson BW. Coding of smooth eye movements in three-dimensional space by frontal cortex. *Nature*. 2002;419(6903):157–162.
13. Akao T, Mustari MJ, Fukushima J, Kurkin S, Fukushima K. Discharge characteristics of pursuit neurons in MST during vergence eye movements. *J Neurophysiol*. 2005;93:2415–2434.
14. Ferraina S, Pare M, Wurtz RH. Disparity sensitivity of frontal eye field neurons. *J Neurophysiol*. 2000;83:625–629.
15. Akao T, Kurkin SA, Fukushima J, Fukushima K. Visual and vergence eye movement related responses of pursuit neurons in the caudal frontal eye fields to motion-in-depth stimuli. *Exp Brain Res*. 2005;164:92–108.
16. Julesz B. *Foundations of Cyclopean Perception*. Chicago, IL: The University of Chicago Press; 1971.
17. Lehmann D, Julesz B. Lateralized cortical potentials evoked in humans by dynamic random-dot stereograms. *Vision Res*. 1978;18(10):1265–1271.
18. Skrandies W. Contrast and stereoscopic visual stimuli yield lateralized scalp potential fields associated with different neural generators. *Electroencephalogr Clin Neurophysiol*. 1991;78(4):274–283.
19. Shen L, Liu Z, Li Y. EEG Based Dynamic RDS Recognition With Frequency Domain Selection and Bispectrum Feature Optimization. *J Neurosci Methods*. 2020;37, 108650.
20. Shen L, Dong X, Li Y. Analysis and classification of hybrid EEG features based on the depth DRDS videos. *J Neurosci Meth*. 2020;38,108690.
21. Teplan M. Fundamentals of EEG measurement. *Meas Sci Rev*. 2002;2:1–11.
22. Stam CJ, Nolte G, Daffertshofer A. Phase Lag Index: Assessment of Functional Connectivity From Multi Channel EEG and MEG With Diminished Bias From Common Sources. *Human Brain Mapping*. 2007;28:1178–1193.
23. Chaturvedi M, Bogaarts JG, Cozac VV, Hatz F, Gschwandtner U, Meyer A, Fuhr P. Volker Roth 3 Phase lag index and spectral power as QEEG features for identification of patients with mild cognitive impairment in Parkinson's disease. *Clin Neurophysiol*. 2019;130(10):1937–1944.

24. Janssen P, Verhoef BE, Premereur E. Functional interaction between the macaque dorsal and ventral visual pathways during three-dimensional object vision. *Cortex*. 2018;98:218–227.
25. Gonzalez DA, Niechwiej-Szwedo E. The effects of monocular viewing on hand-eye coordination during sequential grasping and placing Movements. *Vision Res*. 2016;128:30–38.
26. Fielder AR, Moseley MJ. Does stereopsis matter in human? *Eye*. 1996;10,233–238.
27. Maiello G, Kwon M, Bex PJ. Three-dimensional binocular eye-hand coordination in normal vision and with simulated visual impairment. *Exp Brain Res*. 2018;236(3):691–709.
28. Sloper JJ, Suttle CM, Finlay AL, Melmoth DR, Grant S. Impaired development of eye–hand coordination in children with strabismus and amblyopia. *J Am Assoc Pediatr Ophthalmol Strabismus*. 2011;15(1):e8
29. Ninomiya T, Sawamura H, Inoue K, Takada M. Segregated pathways carrying frontally derived topdown signals to visual areas MT and V4 in macaques. *J Neurosci*. 2012;32:6851–6858.
30. Matsumoto M, Inoue KI, Takada M. Causal Role of Neural Signals Transmitted From the Frontal Eye Field to the Superior Colliculus in Saccade Generation. *Front Neural Circuits*. 2018;28;12:69.
31. Ninomiya T, Sawamura H, Inoue K, Takada M. Segregated pathways carrying frontally derived top-down signals to visual areas MT and V4 in macaques. *J Neurosci*. 2012;32(20):6851–6858.
32. Barcel F, Suwazono S, Knight RT. Prefrontal modulation of visual processing in humans. *Nature Neurosci*. 2000;3:399–403.
33. Yago E, Duarte A, Wong T, Barcel F, Knight RT. Temporal kinetics of prefrontal modulation of the extrastriate cortex during visual attention. *Cognitive, Affective, & Behavioral Neurosci*. 2004;4:609–617.
34. Löwel S, Singer W. Selection of intrinsic horizontal connections in the visual cortex by correlated neuronal activity. *Science*. 1992;255:209–212.
35. Wang T, Li Q, Guo M, et al. Abnormal functional connectivity density in children with anisometropic amblyopia at resting-state. *Brain Res*. 2014;1563C:41–51.
36. Cumming BG, Parker AJ. Responses of primary visual cortical neurons to binocular disparity without depth perception. *Nature*. 1997;389:280–283.
37. Fan L, Li H, Zhuo J, et al. The human brainnetome atlas: A new brain atlas based on connectional architecture. *Cereb Cortex*. 2016;26:3508–3526.
38. Ibrahimi D, Mendiola-Santibañez JD, Cruz-Martínez E, Gómez-Espinosa A, Torres-Pacheco I. Changes in the Brain Activity and Visual Performance of Patients with Strabismus and Amblyopia after a Compete Cycle of Light Therapy. *Brain Sci*. 2021;11:657–677.
39. Li Q, Bai J, Zhang J, et al. Assessment of Cortical Dysfunction in Patients with Intermittent Exotropia: An fMRI Study. *PLoS One*. 2016;11(8):e0160806.
40. Xi S, Yao J, Zhang S, et al. Disrupted neural signals in patients with concomitant exotropia. *Ophthalmic Physiol Opt*. 2020;40(5):650–659.